RSC Advances

PAPER

View Article Online
View Journal | View Issue

Cite this: *RSC Adv.*, 2016, **6**, 55946

Influence of alkyl chain branching point on the electron transport properties of di(perylene diimides) thin film transistors†

Cheng Zeng,[ab] Chengyi Xiao,[b] Rui Xin,[c] Wei Jiang,*[b] Yafei Wang*[a] and Zhaohui Wang[b]

The alkyl chain length and density are fundamental factors affecting solution processability, molecular packing, film microstructure, and charge transport for organic thin film transistors (OTFTs). In this work, four tetra-chlorinated di(perylene diimides) **4CldiPDI-C(1–4)** were prepared through moving the alkyl chain branching position away from the di(perylene diimides) backbone. OTFT devices employing **4CldiPDI-C(1–4)** as the active layer were fabricated. Correspondingly, the effect of the position of the alkyl chain branching point on the film microstructure and charge transport were studied in detail. The research results demonstrate that the different branching point of side-chains has a negligible effect on the absorption maximum and energy gap. Conversely, the gradual movement in the branching point plays a key role in molecular packing and leads to a clear impact on electron mobility ranging from 0.012 to 0.86 $cm^2 V^{-1} s^{-1}$. Therefore, **4CldiPDI-C2**-based devices offered the highest electron mobility of up to 0.86 $cm^2 V^{-1} s^{-1}$ and an on/off ratio of 2×10^7, which is among the best performance of **diPDI** derivatives.

Received 15th April 2016
Accepted 26th May 2016

DOI: 10.1039/c6ra09781b

www.rsc.org/advances

Introduction

Developing n-channel semiconducting materials with high mobility, good processability and air stability is critical for making applicable optoelectronics and constructing complementary logic circuits.[1–9] However, to match the exciting progresses of solution-processed p-channel devices,[10–18] high performance n-channel semiconductors are highly emergent since most of the solution processed n-channel OTFTs exhibit mobilities <0.50 $cm^2 V^{-1} s^{-1}$.[19–28] Additionally, the synthetic inaccessibility and air-unstable charge transporting characteristics limit the further development of n-channel OTFTs.[29] Very recent results showed that many impressive advances have been made by functionalization of π-conjugated backbones such as thiophenes, arylenes and (hetero-)acenes with electron-deficient constituents.[30–32] Nevertheless, few efforts are devoted to exploring the influence of alkyl chains on charge mobilities. In fact, the properties of alkyl chains including alkyl chain length and density have been demonstrated to play an important role on the solution processability, molecular packing, film microstructure, and charge transport.[33–38] Recently, more and more attention has been focused on engineering alkyl chains in small molecules and polymers.[39–42] Compared with linear alkyl chains, branched alkyl chains can bring about better processability and more appropriate crystallinity for large π-conjugated systems.[43–46] Moreover, the branching point will affect the alkyl chain attachment density that has a deep impact on the molecular packing arrangement and determines charge transport behaviour.[47,48] For example, Pei *et al.* demonstrated how moving the branching point away from the isoindigo-based polymer backbone influences the hole mobilities.[47] Furthermore, Zhu *et al.* emphasized branched alkyl chain-dependent molecular packing and charge transport of naphthalene diimide derivatives for enabling high performance solution processed n-channel OTFTs.[48]

It has been widely accepted that perylene diimides (**PDIs**) are a typical class of n-channel organic semiconductors because of their excellent photochemical stability, tunable electronic structure, high electron affinity, and easy chemical modification either at the imide positions or in lateral positions (including *bay* regions and *non-bay* regions) to meet various applications.[49–57] Specially, we have paid attention to the laterally expanded **PDIs** with resulting broadened absorption and lowered LUMO energy levels for achieving high efficient electron transporting materials.[58–61] Accordingly, a series of fully conjugated triply linked oligo(perylene diimides) have been developed, because tetra-chlorinated oligo(perylene diimide) units

[a]*College of Chemistry, Key Lab of Environment-Friendly Chemistry and Application in Ministry of Education, Xiangtan University, Xiangtan 411105, China. E-mail: qiji830404@hotmail.com*

[b]*Key Laboratory of Organic Solids, Beijing National Laboratory for Molecular Sciences, Institute of Chemistry, Chinese Academy of Sciences, Beijing 100190, China. E-mail: jiangwei@iccas.ac.cn*

[c]*State Key Laboratory of Chemical Resource Engineering, Beijing University of Chemical Technology, Beijing 100029, China*

† Electronic supplementary information (ESI) available: Experimental details of the synthesis, characterization, and device fabrication of all materials. See DOI: 10.1039/c6ra09781b

endow the molecules with additional distinct structural characteristics: (i) the expanded π-conjugated aromatic system is expected to induce close intermolecular π–π stacking and achieve efficient electron transport; (ii) four alkyl groups are integrated to the parent molecular framework, which will substantially provide a balance between good solubility, closed intermolecular stacking, and high crystallinity in the thin film state; and (iii) additional tetra-chloro constituents are expected to keep the LUMO levels adequately low to enhance their ambient stability.

In our previous report, we showed that the alkyl chain length of tetra-chlorinated di(perylene diimides) (**4CldiPDIs**) has a significant effect on the electron performances. With an increase of the alkyl chain length, higher electron mobilities could be obtained. Therefore, the linear alkyl chain-substituted **4CldiPDI** showed electron mobilities of 0.011 $cm^2 V^{-1} s^{-1}$ for the *n*-dodecyl substituted-compound (**C12-4CldiPDI**), and 0.70 $cm^2 V^{-1} s^{-1}$ for the *n*-octadecyl-substituted compound (**C18-4CldiPDI**) in air for the thin film devices.[29] Furthermore, we have described our endeavours to study the electron performances of solution processed single crystal transistors based on **C12-4CldiPDI**, which showed an electron mobility as high as 4.65 $cm^2 V^{-1} s^{-1}$, much higher than that based on its film transistors.[62] For the **diPDIs** backbones, we also observed that π-conjugated systems expanded from the doubly linked **PDI** dimer, and triply linked **diPDI**, to the hybrid **NDI-PDI-NDI**, endowing it with uniform branched alkyl chains, which had a significant influence on the molecular packing motifs and thus electron transport properties of the **PDI** derivatives.[63]

An in-depth study on branched alkyl chain-dependent molecular packing and device performance is an interesting but challenging issue, especially for the triply linked **diPDI** systems. In this context, we focused our attention on the influence of moving the alkyl chain branching point from the backbones on the electron transport properties of thin film transistors based on **4CldiPDI** derivatives. Herein, four branched alkyl chains with a gradual change of the branching position were integrated to our **4CldiPDI** systems to produce **4CldiPDI-C1** to **4CldiPDI-C4** with one to four CH_2 spacings, respectively. As the π-conjugated molecular cores became larger and long branched alkyl chains were introduced, it was difficult to achieve a highly crystalline thin film for these molecules. By incorporating alkyl chains with an appropriate branching point, the molecule **4CldiPDI-C2** displays a large area and ordered molecular packing with close intermolecular π–π stacking, and exhibits an exciting electron mobility of up to 0.86 $cm^2 V^{-1} s^{-1}$ and an on/off ratio of 2×10^7. The position of the branching point is confirmed to play the critical role of side-chain engineering in molecular design and contributes to a deeper understanding of the relationship between the molecular structure and the electronic properties.

Experimental

Materials and general methods

All chemicals and solvents were purchased from commercial suppliers and used without further purification unless otherwise specified. The solvent DMSO from Alfa was dry and used directly. Other solvents and common reagents were obtained from the Beijing Chemical Plant. ^{1}H NMR (400 MHz) and ^{13}C NMR (100 MHz) spectra were recorded in deuterated solvents on a Bruker ADVANCE 400 NMR Spectrometer. NMR chemical shifts are reported in ppm using the residual protonated solvent as an internal standard. High resolution mass spectrometry (HRMS) was recorded on an IonSpec 4.7 Tesla Fourier Transform Mass Spectrometer.

Absorption spectra were measured with a Hitachi (model U-3010) UV-vis spectrophotometer in a 1 cm quartz cell. Cyclic voltammetry (CV) was recorded on a Zahner IM6e electrochemical workstation using glassy carbon discs as the working electrode, Pt wire as the counter electrode, and Ag/AgCl electrode as the reference electrode. 0.1 M tetrabutylammonium-hexafluorophosphate (Bu_4NPF_6) dissolved in CH_2Cl_2 (HPLC grade) was employed as the supporting electrolyte, which was calibrated by ferrocene/ferrocenium (Fc/Fc^+) as the redox couple. CH_2Cl_2 was freshly distilled prior to use. TGA measurements were carried out on a PE TGA-7 instrument under a dry nitrogen flow, heating from room temperature to 550 °C, at a heating rate of 10 °C min^{-1}. DSC analyses were performed on TA DSC 2010 instrument under a dry nitrogen flow, heating from room temperature to 300 °C and cooling from 300 °C to room temperature at a rate of 10 °C min^{-1}, 5 °C min^{-1}, or 2 °C min^{-1}. X ray diffraction (XRD) was measured on a D/max 2500 with a Cu Kα source ($\kappa = 1.541$ Å). The films were made on Si wafer substrates. The OFET characteristics were measured in air at room temperature by a Keithley 4200 SCS semiconductor parameter analyzer. In the spin-coating procedure, the rotation speed was 2000 rpm. The mobilities were determined using the following equation: $I_{DS} = (W/2L)C_i\mu(V_{GS} - V_T)^2$. This equation defines the important characters of electron mobility (μ), on/off ratio ($I_{on/off}$), and threshold voltage (V_T), which could be deduced by the equation from a plot of current–voltage.

General synthetic procedure for 4CldiPDI-C(1–4)

4CldiPDI-C(1–4) (Scheme 1) are synthesized and purified based on modified Ullmann reactions according to our previously reported procedures.[49] The mixture of tetra-chloroperylene diimides (**4ClPDIs**) (2.5 mmol), CuI (2.87 g, 15.0 mmol), L-proline (2.01 g, 17.5 mmol), and K_2CO_3 (3.80 g, 27.5 mmol) in 50 mL DMSO was heated at 75 °C under argon for 20 hours. The cooled mixture of solution and solid was poured into water (2000 mL), which was vigorously stirred. Two hours later, the suspension was neutralized with 1 M HCl, then the mixture was stirred for another six hours until the sediment was precipitated completely. After filtration, the filter cake was washed by water and methanol. The cake was dried and purified by column separation (silica gel, PE : DCM = 2 : 1) to get **4CldiPDI-C(1–4)** as purple solids.

4CldiPDI-C1: (268 mg, 10%), ^{1}H NMR (400 MHz, $CDCl_3$): δ = 10.04 (s, 2H, Ph-H), 9.25 (s, 2H, Ph-H), 9.01 (s, 2H, Ph-H), 4.37–4.24 (t, J = 8.0 Hz, 4H, –NCH_2–), 2.32–2.06 (m, 4H, –CH–), 1.47–1.14 (m, 144H, –CH_2–), 0.83–0.78 (m, 24H, –CH_3). ^{13}C NMR (100

MHz, $CDCl_3$): δ = 164.34, 163.27, 162.99, 162.61, 135.95, 135.87, 135.42, 133.87, 132.10, 130.71, 129.85, 128.90, 127.05, 125.91, 125.74, 125.65, 124.57, 124.38, 123.50, 122.04, 121.00, 119.23, 45.72, 45.09, 36.83, 36.67, 32.09, 31.93, 31.91, 31.88, 31.87, 31.81, 30.13, 30.11, 30.08, 29.80, 29.73, 29.71, 29.67, 29.64, 29.40, 29.36, 29.32, 26.87, 26.58, 26.46, 26.26, 22.66, 22.65, 22.64, 22.62, 14.07, 14.03. HRMS (MALDI(N), 100%): calcd (%) for $C_{136}H_{186}Cl_4N_4O_8$, 2146.8040; found 2146.3023.

4CldiPDI-C2: (413 mg, 15%), ^{1}H NMR (400 MHz, $CDCl_3$): δ = 10.06 (s, 2H, Ph-H), 9.25 (s, 2H, Ph-H), 9.01 (s, 2H, Ph-H), 4.42 (t, J = 8.0 Hz, 4H, –NCH_2–), 4.29 (t, J = 8.0 Hz, 4H, –NCH_2–), 1.96–1.76 (m, 8H, –CH–), 1.39–1.20 (m, 148H, –CH_2–), 0.86–0.85 (m, 24H, –CH_3). ^{13}C NMR (100 MHz, $CDCl_3$): δ = 164.04, 163.17, 162.59, 162.31, 135.99, 135.95, 135.32, 133.75, 132.14, 130.81, 129.97, 128.90, 127.05, 126.01, 125.74, 124.58, 124.47, 124.08, 123.60, 122.04, 121.00, 119.13, 40.22, 39.59, 36.13, 33.87, 33.79, 33.68, 33.56, 32.15, 31.94, 30.14, 29.88, 29.78, 29.74, 29.43, 26.73, 26.71, 26.57, 22.73, 22.71, 14.12. HRMS (MALDI(N), 100%): calcd (%) for $C_{140}H_{194}Cl_4N_4O_8$, 2202.9120; found 2203.3671.

4CldiPDI-C3: (339 mg, 12%), ^{1}H NMR (400 MHz, $CDCl_3$): δ = 10.07 (s, 2H, Ph-H), 9.27 (s, 2H, Ph-H), 9.01 (s, 2H, Ph-H), 4.41 (t, J = 8.0 Hz, 4H, –NCH_2–), 4.27 (t, J = 8.0 Hz, 4H, –NCH_2–), 1.97–1.80 (m, 8H, –CH–), 1.50–1.20 (m, 156H, –CH_2–), 0.84–0.82 (m, 24H, –CH_3). ^{13}C NMR (100 MHz, $CDCl_3$): δ = 164.26, 163.22, 162.69, 162.31, 135.99, 135.95, 135.32, 133.85, 132.24, 130.91, 129.97, 128.90, 127.05, 126.11, 125.74, 124.58, 124.37, 124.18, 123.60, 122.04, 121.00, 119.13, 42.42, 41.59, 37.33, 33.67, 33.59, 31.98, 31.16, 30.15, 29.74, 29.63, 29.33, 26.81, 26.77, 26.74, 25.56, 22.73, 14.12. HRMS (MALDI(N), 100%): calcd (%) for $C_{144}H_{202}Cl_4N_4O_8$, 2259.0200; found 2258.4305.

4CldiPDI-C4: (318 mg, 11%), ^{1}H NMR (400 MHz, $CDCl_3$): δ = 10.07 (s, 2H, Ph-H), 9.27 (s, 2H, Ph-H), 9.01 (s, 2H, Ph-H), 4.45 (t, J = 8.0 Hz, 4H, –NCH_2–), 4.28 (t, J = 8.0 Hz, 4H, –NCH_2–), 1.97–1.80 (m, 8H, –CH–), 1.35–1.21 (m, 156H, –CH_2–), 0.87–0.83 (m, 24H, –CH_3). ^{13}C NMR (100 MHz, $CDCl_3$): δ = 164.26, 163.22, 162.69, 162.31, 136.09, 136.05, 135.32, 133.85, 132.14, 130.91, 129.97, 128.90, 127.05, 126.11, 125.74, 124.58, 124.47, 124.08, 123.60, 122.04, 121.00, 119.13, 42.02, 41.29, 37.53, 37.43, 33.67, 33.59, 31.98, 30.25, 29.74, 29.63, 29.33, 28.75, 28.61, 26.77, 24.56, 22.73, 14.15. HRMS (MALDI(N), 100%): calcd (%) for $C_{148}H_{210}Cl_4N_4O_8$, 2315.1280; found 2314.4932.

Results and discussion

Optical, electrochemical and thermal properties

The UV-vis absorption spectra of the four compounds **4CldiPDI-C(1–4)** in $CHCl_3$ solution are shown in Fig. 1. They all exhibit broad absorption bands up to the near-infrared region with high extinction coefficients. The absorption spectra are almost identical suggesting that the alkyl chains on the *N*-positions do not affect the optical properties of the whole aromatic core. All compounds showed major absorption bands at 654, 600, 546, 506, and 408 nm. And optical band gaps of about 1.84 eV were estimated from the onset absorption wavelengths of around 675 nm. The absorption intensity is slightly decreased on

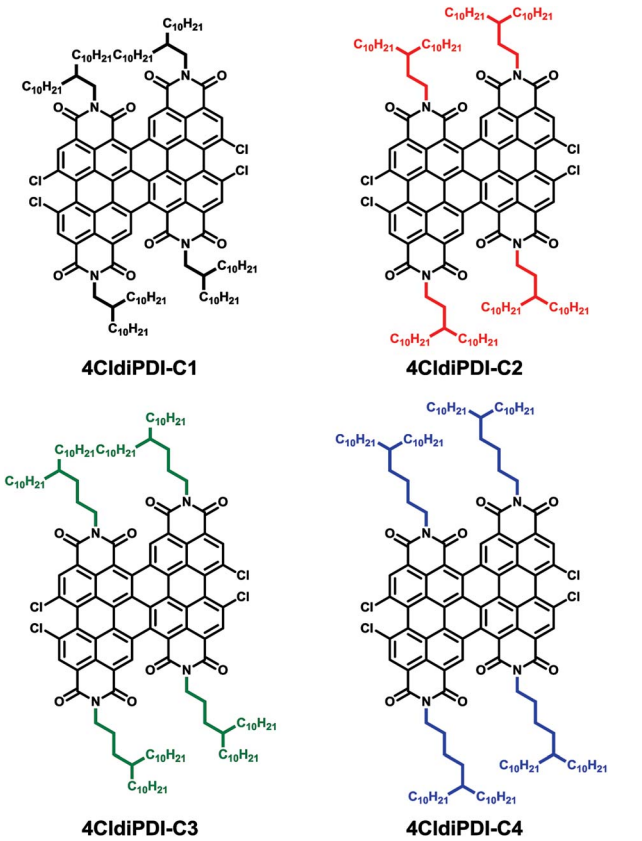

Scheme 1 Molecular structures of **4CldiPDI-C(1–4)** with varying branch positions of the alkyl side-chains.

lengthening the alkyl chains on the *N*-positions from **4CldiPDI-C1** to **4CldiPDI-C4** (Table 1).

Electrochemical analysis of **4CldiPDI-C(1–4)** was carried out using cyclic voltammetry (CV) in 0.1 M Bu_4NPF_6–CH_2Cl_2 solutions with a scan rate of 100 mV s^{-1}. All compounds showed well-defined, single-electron, two reversible and two quasi-reversible reduction peaks. The half-wave reduction potentials *vs.* Fc/Fc^+, as well as the LUMO levels estimated from the onset of reduction potentials (−0.54 V), are summarized in Table 1. Their LUMO levels almost reach −4.26 eV, hinting at ambient-stable electron transport n-channel OTFT semiconductors. Both the UV-vis spectra and CV results have shown that the alkyl chain branching point had little influence on the photophysical properties.

The thermal properties of **4CldiPDI-C(1–4)** were evaluated by thermogravimetric analysis (TGA) and differential scanning calorimetry (DSC). Their 5% weight loss temperatures (T_{deg}) are listed in Table 1 and Fig. S1,† proving that all the compounds are thermally stable with a decomposition temperature up to 370 °C under a nitrogen atmosphere.

The thermotropic behavior was investigated by DSC measurement with a TA Instruments apparatus. The DSC images are shown in Fig. 2. Phase transition temperatures were determined during the second heating cycle at a scanning rate of 10 K min^{-1} (except **4CldiPDI-C1**, performed at 2 K min^{-1}). The first heating cycles of DSC were neglected to exclude

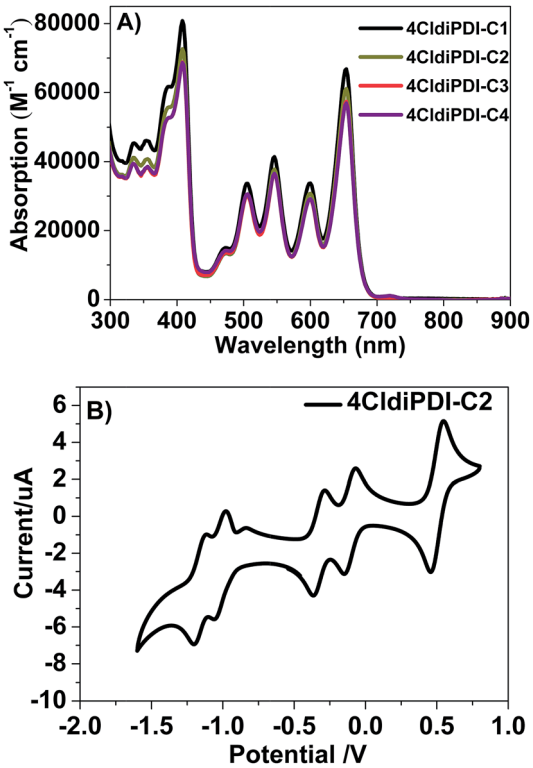

Fig. 1 (A) UV-vis absorption spectra of compounds **4CldiPDI-C(1–4)** in $CHCl_3$ solution and (B) cyclic voltammogram of compound **4CldiPDI-C2** in CH_2Cl_2 solution.

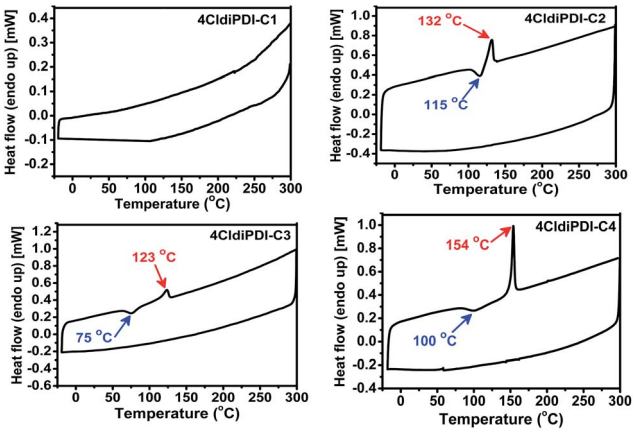

Fig. 2 DSC plots of **4CldiPDI-C(1–4)**.

influences of the thermal history of the samples. No matter whether a scanning rate of 10 K min^{-1}, 5 K min^{-1} or 2 K min^{-1} was used, it was always hard to get a clear melting peak and freezing peak for **4CldiPDI-C1** featuring the nearest branching point, hinting at its disordered structure. Meanwhile, the melting peaks (T_m) of 132 °C, 123 °C, and 154 °C for **4CldiPDI-C(2–4)** are sharper, exhibiting more reversible thermal transitions, suggesting their more ordered and crystalline structures. It should be noted that the first transition peaks at 115 °C, 75 °C, and 100 °C, respectively, for compounds **4CldiPDI-C(2–4)** correspond to a crystalline–crystalline transition.[64] **4CldiPDI-C4** possessed the furthest branching point and therefore exhibited the highest melting point of 154 °C, which was opposite to the longer alkyl chain usually resulting in a lower clearing temperature.[65] Compound **4CldiPDI-C3** instead of **4CldiPDI-C2** got the lowest melting point; this phenomenon may be caused by the odd-even oscillation. It is a well studied and understood concept that the even spacer can pack more efficiently compared to the odd one. The highly packed structure requires more energy for melting and similarly releases more energy while crystallizing as compared to the weakly packed molecules. It is reflected in the melting temperature as well as the crystalline–crystalline transition temperature that the even CH_2 spacings have a higher temperature. The four compounds do not recrystallize on cooling, probably because of the lengthy alkyl chains on the *N*-positions,[66] and no evidence was detected for a liquid-crystalline phase transition for all the **4CldiPDIs**.

OFET characteristics

The good solubility of **4CldiPDI-C(1–4)** in organic solvents promised excellent film properties by spin-coating techniques. The thin films of **4CldiPDI-C(1–4)** with a thickness of 40–60 nm were prepared on the substrates in air by spin-coating from their $CHCl_3$ solution (10 mg mL^{-1}). The substrates were modified by *n*-octadecyl trimethoxysilane (OTS) on the surface of the SiO_2/Si substrate. Here, the OTS-modified SiO_2 layer was used as the dielectric layer, with a capacitance of 10 nF cm^{-2}. The Au source–drain electrodes (30 nm thick) were sputtered and patterned by a lift-off technique,[46] affording a channel length (L) and width (W) of these bottom-gate bottom-contact (BGBC) OTFTs of 50 μm and 1400 μm respectively. In order to discover the effect of the position of the branched alkyl chains on the mobility among these compounds with the same aromatic core,

Table 1 Optical, electrochemical and thermal properties of **4CldiPDI-C(1–4)**

Compounds	λ_{max}[a] (nm)	ε[a] (M^{-1} cm^{-1})	E_g[b] (eV)	E_{LUMO}[c] (eV)	E_{HOMO}[d] (eV)	T_{deg}[e] (°C)
4CldiPDI-C1	654	66 826	1.84	−4.26	−6.10	393
4CldiPDI-C2	654	61 078	1.84	−4.26	−6.10	375
4CldiPDI-C3	654	57 401	1.84	−4.26	−6.10	384
4CldiPDI-C4	654	56 926	1.84	−4.26	−6.10	386

[a] Measured in dilute $CHCl_3$ solution (1.0×10^5 M). [b] Calculated by the onset of absorption in $CHCl_3$ solution according to $E_g = (1240/\lambda_{onset})$. [c] LUMO (eV) estimated by the onset of reduction peaks and calculated according to E_{LUMO} (eV) $= -(4.8 + E_{onset})$. [d] Calculated according to $E_{HOMO} = -(E_g - E_{LUMO})$ eV. [e] Decomposition temperature determined by TGA corresponding to 5% weight loss at 10 °C min^{-1} under nitrogen flow.

we designed comparative experiments for each of them at different annealing temperatures. The compound with the highest mobility at the optimal annealing temperature was expected to be found. Table 2 summarizes the OFET characteristics of the devices evaluated under ambient conditions.

For the BGBC device geometry, a similar trend of branched alkyl chain-dependent mobility can be clearly observed. The four compounds exhibit optimal mobilities of 0.012, 0.86, 0.18, and 0.10 $cm^2 V^{-1} s^{-1}$, respectively, while **4CldiPDI-C2** shows the best electron transporting performances with a mobility of up to 0.86 $cm^2 V^{-1} s^{-1}$, which is much higher than that of the **C12-4CldiPDI** (0.011 $cm^2 V^{-1} s^{-1}$) and **C18-4CldiPDI** (0.7 $cm^2 V^{-1} s^{-1}$) based film devices. Since the difference in the side-chain length and the position of branching point constitutes the only difference for these n-channel semiconductors, it implies that the nature of the branched alkyl substituents has a profound impact on the device performance of these **4CldiPDI** derivatives.

To further investigate the side-chain effect on the device performances, we studied the dependence of the mobilities of the **4CldiPDI-C(1–4)** devices on the annealing temperatures. In Fig. 3, as for **4CldiPDI-C2** when the annealing temperature increased, the mobilities increased smoothly from ~0.08 to ~0.86 $cm^2 V^{-1} s^{-1}$. High mobilities of 0.5 and 0.86 $cm^2 V^{-1} s^{-1}$ can be achieved after annealing at 120 and 140 °C, respectively, which indicates that **4CldiPDI-C2** possess potential for use in flexible electronic applications. The mobilities of the **4CldiPDI-C1**- and **4CldiPDI-C3**-based OTFTs steadily increased for annealing temperatures up to 80 °C. When the annealing temperature was >80 °C, the electron mobilities increased dramatically. In particular, the mobilities improved by an order of magnitude. **4CldiPDI-C4** was similar to **4CldiPDI-C2**, and the mobilities increased steadily, but with annealing temperatures up to 100 °C, the mobilities improved dramatically to a maximum value of 0.10 $cm^2 V^{-1} s^{-1}$ (Table S1†).

The output and transfer characteristics based on semiconductors of compounds **4CldiPDI-C(1–4)** are shown in Fig. S4 and S5 (ESI†). All compounds showed obvious n-channel behaviour with a good line and saturation region. And the electron mobilities got better on increasing the annealing temperature, but if the annealing temperature was further raised, we can't get significant mobility, which can be reflected by DSC, XRD and AFM. We speculated that this phenomenon was due to their relatively low melting points, although the annealing temperature did not exceed the T_m of such compounds. The crystalline structure of films was damaged under higher annealing conditions, resulting in an expected decreased performance.

Table 2 Optimized device performance of OTFTs based on 4CldiPDI-C(1–4) at optimized annealing temperatures in air

Compounds	T^a (°C)	Mobility ($cm^2 V^{-1} s^{-1}$)	V_T (V)	On/off ratio
4CldiPDI-C1	110	0.012	0.3	6×10^4
4CldiPDI-C2	140	0.86	1.29	2×10^7
4CldiPDI-C3	120	0.18	−3.6	6×10^5
4CldiPDI-C4	120	0.10	0.5	8×10^4

[a] Annealing at this temperature for 10 min.

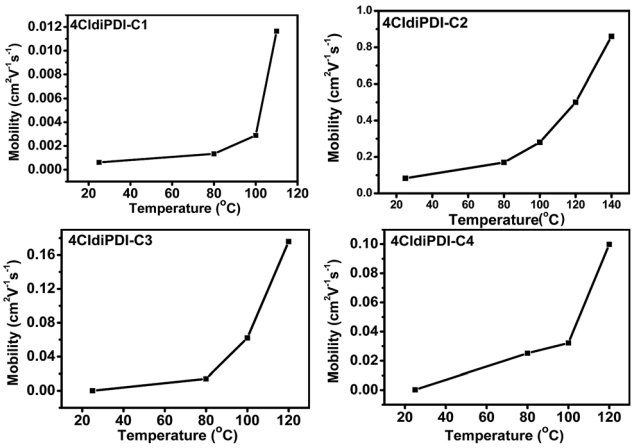

Fig. 3 Device mobility of the 4CldiPDI-C(1–4)-based OTFTs as a function of annealing temperature.

Thin film morphology

From the DSC curves, we got the temperatures of the crystalline–crystalline transition and melting point of **4CldiPDI-C(1–4)**. Fig. S3 (ESI†) shows the lab-based specular XRD patterns of thin films of all the compounds, and the thin films of **4CldiPDI-C2** and **4CldiPDI-C4** exhibit sharp Bragg reflections up to the third or fourth order, suggesting a high degree of crystallinity, but **4CldiPDI-C1** and **4CldiPDI-C3** did not. For **4CldiPDI-C2** and **4CldiPDI-C4**, an obvious phase transition indicated by the change in *d*-spacing with the variation of temperatures can be observed for the thin films.

When heating, the peak of **4CldiPDI-C4** corresponding to a *d*-spacing of 3.16 nm shifts to 3.53 nm with the temperature above 140 °C, then the temperature cooled to 100 °C, with the reflection corresponding to a *d*-spacing at 3.45 nm, and the peaks are very sharp. In the case of **4CldiPDI-C2**, the peaks are without significant change until the temperature exceed 160 °C, at which the compound had melted. But on cooling to 130 °C, a peak appeared and the peak corresponded to a *d*-spacing of 3.13 nm. When the temperature was lowered to 120 °C the compound exhibited two different phases with a *d*-spacing distance of 3.11 and 2.45 nm, respectively, indicating that a phase transition occurred during thermal treatment.

From the AFM images in Fig. 4, we have found that thin films of **4CldiPDI-C2** exhibit a temperature-dependent morphology: crystalline grains become bigger and grain boundaries get larger as the temperature elevated, agreeing with the variation of mobilities, and obvious morphology changes occur at an annealing temperature of 120 °C. And this phenomenon can also be reflected with XRD as shown in the ESI, Fig. S3,† which indicates more intense *d*-spacing peaks in line with the increased temperatures. Upon thermal annealing at the optimized temperatures of the four compounds (ESI, Fig. S2†), the terraces of the **4CldiPDI-C2** films are remarkably large and smooth. This is an indication of highly ordered molecular

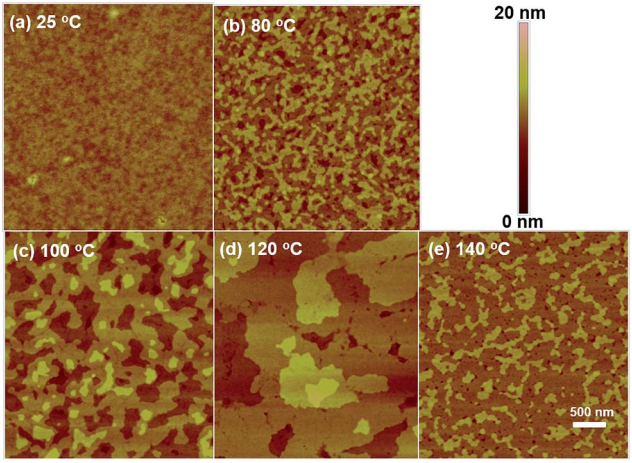

Fig. 4 Comparison of AFM images of thin films of **4CldiPDI-C2** at different annealing temperatures.

packing within the film and might be a result of the triply linked **diPDI** core with four branched alkyl substituents.

Conclusions

In conclusion, we have demonstrated a family of **4CldiPDIs** having branched *N*-alkyl chains with different side-chain lengths and positions of the branching point to study their charge transport properties. The focus of investigation was directed toward designing different branching points of the side-chain of the **diPDIs** and to elucidate a structure–property relationship with respect to the charge transport properties in *N*-substituted derivatives of **diPDIs**. To this end, the four compounds are suitable for solution processability, implying their superior solubility in organic solvents. Thermal, optical, and electrochemical properties are measured by UV-vis absorption spectra, DSC, TGA, and cyclic voltammetry measurements. To investigate the thin film field effect properties of the series of materials, a bottom-gate bottom-contact device configuration was afforded. The subtle changes in the position of the branching point lead to significant differences in both the molecular packing and film morphology, resulting in nearly two orders of magnitude of variation in electron mobility. The four compounds exhibit optimized mobilities of 0.012, 0.86, 0.18, and 0.10 $cm^2\ V^{-1}\ s^{-1}$, respectively. Especially, **4CldiPDI-C2** films possess efficient in-plane packing and large grain sizes enabling an exciting electron mobility of up to 0.86 $cm^2\ V^{-1}\ s^{-1}$, which is a record value for the family of **diPDI** derivatives. Preliminary results demonstrated that the branched side-chains are important for both molecular packing and film morphology. It is often possible to design organic semiconducting materials such that effective charge transport appears by choosing appropriate substituents.

Acknowledgements

For financial support of this research, we thank 973 Program (Grant 2013CB933503), the National Natural Science Foundation of China (21225209, 21190032, and 91427303), NSFC-DFG Joint Project TRR61, and the Chinese Academy of Sciences (XDB12010000).

Notes and references

1 Y. Wen, Y. Liu, Y. Guo, G. Yu and W. Hu, *Chem. Rev.*, 2011, **111**, 3358–3406.
2 C. Li and H. Wonneberger, *Adv. Mater.*, 2012, **24**, 613–636.
3 X. Zhan, A. Facchetti, S. Barlow, T. J. Marks, M. A. Ratner, M. R. Wasielewski and S. R. Marder, *Adv. Mater.*, 2011, **23**, 268–284.
4 L. Schmidt-Mende, A. Fechtenkotter, K. Mullen, E. Moons, R. H. Friend and J. D. MacKenzie, *Science*, 2001, **293**, 1119–1122.
5 M. Gsanger, D. Bialas, L. Huang, M. Stolte and F. Wurthner, *Adv. Mater.*, 2016, **28**, 3615–3645.
6 Q. Yan, Z. Luo, K. Cai, Y. Ma and D. Zhao, *Chem. Soc. Rev.*, 2014, **43**, 4199–4221.
7 K. Shi, F. Zhang, C. A. Di, T. W. Yan, Y. Zou, X. Zhou, D. Zhu, J. Y. Wang and J. Pei, *J. Am. Chem. Soc.*, 2015, **137**, 6979–6982.
8 A. N. Sokolov, B. C. Tee, C. J. Bettinger, J. B. Tok and Z. Bao, *Acc. Chem. Res.*, 2012, **45**, 361–371.
9 H. Usta, A. Facchetti and T. J. Marks, *Acc. Chem. Res.*, 2011, **44**, 501–510.
10 A. Hamaguchi, T. Negishi, Y. Kimura, Y. Ikeda, K. Takimiya, S. Z. Bisri, Y. Iwasa and T. Shiro, *Adv. Mater.*, 2015, **27**, 6606–6611.
11 H. Minemawari, T. Yamada, H. Matsui, J. Tsutsumi, S. Haas, R. Chiba, R. Kumai and T. Hasegawa, *Nature*, 2011, **475**, 364–367.
12 H. Chen, Y. Guo, G. Yu, Y. Zhao, J. Zhang, D. Gao, H. Liu and Y. Liu, *Adv. Mater.*, 2012, **24**, 4618–4622.
13 K. Nakayama, Y. Hirose, J. Soeda, M. Yoshizumi, T. Uemura, M. Uno, W. Li, M. J. Kang, M. Yamagishi, Y. Okada, E. Miyazaki, Y. Nakazawa, A. Nakao, K. Takimiya and J. Takeya, *Adv. Mater.*, 2011, **23**, 1626–1629.
14 J. Smith, W. Zhang, R. Sougrat, K. Zhao, R. Li, D. Cha, A. Amassian, M. Heeney, I. McCulloch and T. D. Anthopoulos, *Adv. Mater.*, 2012, **24**, 2441–2446.
15 G. Giri, E. Verploegen, S. C. Mannsfeld, S. Atahan-Evrenk, H. Kim do, S. Y. Lee, H. A. Becerril, A. Aspuru-Guzik, M. F. Toney and Z. Bao, *Nature*, 2011, **480**, 504–508.
16 H. N. Tsao, D. M. Cho, I. Park, M. R. Hansen, A. Mavrinskiy, Y. Yoon do, R. Graf, W. Pisula, H. W. Spiess and K. Mullen, *J. Am. Chem. Soc.*, 2011, **133**, 2605–2612.
17 L. Zhang, A. Fonari, Y. Liu, A. L. Hoyt, H. Lee, D. Granger, S. Parkin, T. P. Russell, J. E. Anthony, J. L. Bredas, V. Coropceanu and A. L. Briseno, *J. Am. Chem. Soc.*, 2014, **136**, 9248–9251.
18 H. J. Yun, G. B. Lee, D. S. Chung, Y. H. Kim and S. K. Kwon, *Adv. Mater.*, 2014, **26**, 6612–6616.
19 H. Yan, Z. Chen, Y. Zheng, C. Newman, J. R. Quinn, F. Dotz, M. Kastler and A. Facchetti, *Nature*, 2009, **457**, 679–686.
20 X. Gao, C. A. Di, Y. Hu, X. Yang, H. Fan, F. Zhang, Y. Liu, H. Li and D. Zhu, *J. Am. Chem. Soc.*, 2010, **132**, 3697–3699.

21 L. E. Polander, S. P. Tiwari, L. Pandey, B. M. Seifried, Q. Zhang, S. Barlow, C. Risko, J.-L. Brédas, B. Kippelen and S. R. Marder, *Chem. Mater.*, 2011, **23**, 3408–3410.
22 Y. Zhao, C. A. Di, X. Gao, Y. Hu, Y. Guo, L. Zhang, Y. Liu, J. Wang, W. Hu and D. Zhu, *Adv. Mater.*, 2011, **23**, 2448–2453.
23 Y. Hu, Y. Qin, X. Gao, F. Zhang, C. A. Di, Z. Zhao, H. Li and D. Zhu, *Org. Lett.*, 2012, **14**, 292–295.
24 Y. Qiao, Y. Guo, C. Yu, F. Zhang, W. Xu, Y. Liu and D. Zhu, *J. Am. Chem. Soc.*, 2012, **134**, 4084–4087.
25 H. Zhong, J. Smith, S. Rossbauer, A. J. White, T. D. Anthopoulos and M. Heeney, *Adv. Mater.*, 2012, **24**, 3205–3211.
26 C. Zhang, Y. Zang, E. Gann, C. R. McNeill, X. Zhu, C. A. Di and D. Zhu, *J. Am. Chem. Soc.*, 2014, **136**, 16176–16184.
27 M. Mamada, H. Shima, Y. Yoneda, T. Shimano, N. Yamada, K. Kakita, T. Machida, Y. Tanaka, S. Aotsuka, D. Kumaki and S. Tokito, *Chem. Mater.*, 2015, **27**, 141–147.
28 M. Nakano, I. Osaka, D. Hashizume and K. Takimiya, *Chem. Mater.*, 2015, **27**, 6418–6425.
29 J. Zhang, L. Tan, W. Jiang, W. Hu and Z. Wang, *J. Mater. Chem. C*, 2013, **1**, 3200.
30 R. Schmidt, J. H. Oh, Y. S. Sun, M. Deppisch, A. M. Krause, K. Radacki, H. Braunschweig, M. Konemann, P. Erk, Z. Bao and F. Wurthner, *J. Am. Chem. Soc.*, 2009, **131**, 6215–6228.
31 H. E. Katz, A. J. Lovinger, J. Johnson, C. Kloc, T. Siegrist, W. Li, Y. Y. Lin and A. Dodabalapur, *Nature*, 2000, **404**, 478–481.
32 Z. Liu, G. Zhang, Z. Cai, X. Chen, H. Luo, Y. Li, J. Wang and D. Zhang, *Adv. Mater.*, 2014, **26**, 6965–6977.
33 H. Sirringhaus, P. J. Brown, R. H. Friend, M. M. Nielsen, K. Bechgaard, B. M. W. Langeveld-Voss, A. J. H. Spiering, R. A. J. Janssen, E. W. Meijer, P. Herwig and D. M. de Leeuw, *Nature*, 1999, **401**, 685–688.
34 I. McCulloch, M. Heeney, C. Bailey, K. Genevicius, I. Macdonald, M. Shkunov, D. Sparrowe, S. Tierney, R. Wagner, W. Zhang, M. L. Chabinyc, R. J. Kline, M. D. McGehee and M. F. Toney, *Nat. Mater.*, 2006, **5**, 328–333.
35 R. J. Kline, D. M. DeLongchamp, D. A. Fischer, E. K. Lin, L. J. Richter, M. L. Chabinyc, M. F. Toney, M. Heeney and I. McCulloch, *Macromolecules*, 2007, **40**, 7960–7965.
36 M. T. Stone, J. M. Heemstra and J. S. Moore, *Acc. Chem. Res.*, 2006, **39**, 11–20.
37 K. Nakayama, Y. Hirose, J. Soeda, M. Yoshizumi, T. Uemura, M. Uno, W. Li, M. J. Kang, M. Yamagishi, Y. Okada, E. Miyazaki, Y. Nakazawa, A. Nakao, K. Takimiya and J. Takeya, *Adv. Mater.*, 2011, **23**, 1626–1629.
38 S. Ogi, V. Stepanenko, J. Thein and F. Wurthner, *J. Am. Chem. Soc.*, 2016, **138**, 670–678.
39 A. L. Ayzner, J. Mei, A. Appleton, D. DeLongchamp, A. Nardes, S. Benight, N. Kopidakis, M. F. Toney and Z. Bao, *ACS Appl. Mater. Interfaces*, 2015, **7**, 28035–28041.
40 T. Wohrle, I. Wurzbach, J. Kirres, A. Kostidou, N. Kapernaum, J. Litterscheidt, J. C. Haenle, P. Staffeld, A. Baro, F. Giesselmann and S. Laschat, *Chem. Rev.*, 2016, **116**, 1139–1241.
41 F. Wurthner, C. R. Saha-Moller, B. Fimmel, S. Ogi, P. Leowanawat and D. Schmidt, *Chem. Rev.*, 2016, **116**, 962–1052.
42 I. Kang, H.-J. Yun, D. S. Chung, S.-K. Kwon and Y.-H. Kim, *J. Am. Chem. Soc.*, 2013, **135**, 14896–14899.
43 L. Zhang, Y. Cao, N. S. Colella, Y. Liang, J. L. Bredas, K. N. Houk and A. L. Briseno, *Acc. Chem. Res.*, 2015, **48**, 500–509.
44 P. Duan, N. Yanai and N. Kimizuka, *J. Am. Chem. Soc.*, 2013, **135**, 19056–19059.
45 W. S. Yoon, S. K. Park, I. Cho, J.-A. Oh, J. H. Kim and S. Y. Park, *Adv. Funct. Mater.*, 2013, **23**, 3519–3524.
46 X. Guo, F. S. Kim, M. J. Seger, S. A. Jenekhe and M. D. Watson, *Chem. Mater.*, 2012, **24**, 1434–1442.
47 T. Lei, J. H. Dou and J. Pei, *Adv. Mater.*, 2012, **24**, 6457–6461.
48 F. Zhang, Y. Hu, T. Schuettfort, C. A. Di, X. Gao, C. R. McNeill, L. Thomsen, S. C. Mannsfeld, W. Yuan, H. Sirringhaus and D. Zhu, *J. Am. Chem. Soc.*, 2013, **135**, 2338–2349.
49 H. Qian, Z. Wang, W. Yue and D. Zhu, *J. Am. Chem. Soc.*, 2007, **129**, 10664–10665.
50 H. Qian, F. Negri, C. Wang and Z. Wang, *J. Am. Chem. Soc.*, 2008, **130**, 17970–17976.
51 Y. Zhen, C. Wang and Z. Wang, *Chem. Commun.*, 2010, **46**, 1926–1928.
52 Y. Li, L. Tan, Z. Wang, H. Qian, Y. Shi and W. Hu, *Org. Lett.*, 2008, **10**, 529–532.
53 C. Ego, D. Marsitzky, S. Becker, J. Zhang, A. C. Grimsdale, K. Mullen, J. D. MacKenzie, C. Silva and R. H. Friend, *J. Am. Chem. Soc.*, 2003, **125**, 437–443.
54 X. Zhan, Z. A. Tan, B. Domercq, Z. An, X. Zhang, S. Barlow, Y. Li, D. Zhu, B. Kippelen and S. R. Marder, *J. Am. Chem. Soc.*, 2007, **129**, 7246–7247.
55 S. Chen, P. Slattum, C. Wang and L. Zang, *Chem. Rev.*, 2015, **115**, 11967–11998.
56 D. Meng, D. Sun, C. Zhong, T. Liu, B. Fan, L. Huo, Y. Li, W. Jiang, H. Choi, T. Kim, J. Y. Kim, Y. Sun, Z. Wang and A. J. Heeger, *J. Am. Chem. Soc.*, 2016, **138**, 375–380.
57 D. Zhao, Q. Wu, Z. Cai, T. Zheng, W. Chen, J. Lu and L. Yu, *Chem. Mater.*, 2016, **28**, 1139–1146.
58 W. Jiang, Y. Li and Z. Wang, *Acc. Chem. Res.*, 2014, **47**, 3135–3147.
59 W. Jiang, L. Ye, X. Li, C. Xiao, F. Tan, W. Zhao, J. Hou and Z. Wang, *Chem. Commun.*, 2014, **50**, 1024–1026.
60 H. Qian, C. Liu, Z. Wang and D. Zhu, *Chem. Commun.*, 2006, 4587–4589.
61 W. Jiang, Y. Li, W. Yue, Y. Zhen, J. Qu and Z. Wang, *Org. Lett.*, 2010, **12**, 228–231.
62 A. Lv, S. R. Puniredd, J. Zhang, Z. Li, H. Zhu, W. Jiang, H. Dong, Y. He, L. Jiang, Y. Li, W. Pisula, Q. Meng, W. Hu and Z. Wang, *Adv. Mater.*, 2012, **24**, 2626–2630.
63 C. Xiao, W. Jiang, X. Li, L. Hao, C. Liu and Z. Wang, *ACS Appl. Mater. Interfaces*, 2014, **6**, 18098–18103.
64 T. Zhang, D. Sun, X. Ren, L. Liu, G. Wen, Z. Ren, H. Li and S. Yan, *Soft Matter*, 2013, **9**, 10739.
65 A. Wicklein, A. Lang, M. Muth and M. Thelakkat, *J. Am. Chem. Soc.*, 2009, **131**, 14442–14453.
66 C. Cuerva, J. A. Campo, P. Ovejero, M. R. Torres, E. Oliveira, S. M. Santos, C. Lodeiro and M. Cano, *J. Mater. Chem. C*, 2014, **2**, 9167–9181.

